

# High-quality Image Deblurring with Panchromatic Pixels

Sen Wang  
Eastman Kodak Company  
Tingbo Hou  
Stony Brook University  
John Border  
Eastman Kodak Company  
Hong Qin  
Stony Brook University  
and  
Rodney Miller  
Eastman Kodak Company

Image deblurring is a very challenging problem in recent decades. In this paper, we propose a high-quality image deblurring method with a novel image prior based on a new imaging system. The imaging system has a newly designed sensor pattern by adding panchromatic (pan) pixels to the conventional Bayer pattern. Since these pan pixels are sensitive to all wavelengths of visible light, they collect a significantly higher proportion of the light striking the sensor. A new demosaicing algorithm is also proposed to restore full-resolution images from pixels on the sensor. The shutter speed of pan pixels is controllable to users. Therefore, we can have multiple images with different exposures. When long exposure is needed under dim light, we read pan pixels twice in one shot: one with short exposure and the other with long exposure. The long-exposure image is often blurred, while the short-exposure image can be sharp and noisy. The short-exposure image plays an important role in deblurring, since it is sharp and there is no alignment problem for the one-shot image pair. For the algorithmic aspect, our method runs in a two-step Maximum-a-Posteriori (MAP) fashion under a joint minimization of the blur kernel and the deblurred image. The algorithm exploits a combined image prior including a statistical part and a spatial part, which is powerful in ringing controls. Extensive experiments under various conditions and settings are conducted to demonstrate the performance of our method.

Categories and Subject Descriptors: I.3.3 [Computer Graphics]: Picture/Image Generation—*Digitizing and scanning*; I.4.3 [Computer

**Graphics**]: Image Processing and Computer Vision—*Sharpening and deblurring*

General Terms: Smart Image Sensor, Image Deblurring

Additional Key Words and Phrases: Panchromatic Pixel, Image Deconvolution, Motion Deblurring, Ringing Control

**ACM Reference Format:**

Wang, S., Hou, T., Border, J., Qin, H., and Miller, R. 2010.

## 1. INTRODUCTION

Image deblurring has been studied for decades with impressive progress accomplished recently, yet it still remains active and challenging in terms of high-quality and generality. In essence, it is an inverse problem with more unknown variables than the number of equations. The inference of latent sharp images with inadequate information can easily lead to unwanted solutions. Recent research reveals an effective strategy to address this challenge, which is to solve the small-sized blur kernel first, and then estimate the latent image [Levin et al. 2009]. Following this paradigm, techniques and tools were invented, including image priors for regularization and specially-designed camera systems that can acquire more information. This accomplishment inspires us to design a new imaging system and a novel image prior.

Many approaches were proposed for recovering the sharp latent image from a single blurred image. The recent work [Fergus et al. 2006; Shan et al. 2008] usually addressed this problem using regularization based on the *natural image prior*. It refers to the heavy-tailed distribution of gradient magnitudes for natural images. This prior favors solutions with fewer large gradients, and therefore, reduces ringing artifacts. However, these methods may cause the maximum-a-posteriori (MAP) failure [Levin et al. 2009]. That is, the inference may get stuck at the starting place, since the delta kernel is also favored by the natural image prior. The methods often carry out estimations of the blur kernel and the latent image iteratively. Without further information in regularization, it is possible to produce severe ringing artifacts by small errors from the iterative procedure.

New imaging system design plays a fundamental and critical role in high-quality deblurring, which can afford more information

---

Authors' addresses: land and/or email addresses.

Permission to make digital or hard copies of part or all of this work for personal or classroom use is granted without fee provided that copies are not made or distributed for profit or commercial advantage and that copies show this notice on the first page or initial screen of a display along with the full citation. Copyrights for components of this work owned by others than ACM must be honored. Abstracting with credit is permitted. To copy otherwise, to republish, to post on servers, to redistribute to lists, or to use any component of this work in other works requires prior specific permission and/or a fee. Permissions may be requested from Publications Dept., ACM, Inc., 2 Penn Plaza, Suite 701, New York, NY 10121-0701 USA, fax +1 (212) 869-0481, or [permissions@acm.org](mailto:permissions@acm.org).

© YYYY ACM 0730-0301/YYYY/11-ARTXXX \$10.00

DOI 10.1145/XXXXXXX.YYYYYYY

<http://doi.acm.org/10.1145/XXXXXXX.YYYYYYY>

rather than blurry scenes. Image sensors with rapid responses to light can instantly reduce motion blurs. However, consumer sensors still need long-time exposure for photon collection under circumstances such as dim light, where the captured photos are blurred. Researchers endeavor to design image deblurring systems with special cameras that can provide multiple images with different shutter speeds [Ben-Ezra and Nayar 2003; Raskar et al. 2006; Lim and Silverstein 2006; Yuan et al. 2007]. Images with slow shutter speeds are often blurred, while the ones with fast shutter speeds could be sharp and noisy. There are some characteristics about the imaging systems that may affect the quality of deblurring:

- (1) **Alignment.** The spatial and temporal displacements caused by multiple lenses and multiple shots are very common in a multi-image system. However, the alignment of blurry images is hard to carried out due to the ambiguity between blurs and displacements. Therefore, from the alignment's point of view, one shot is better than multiple shots in principle.
- (2) **Shutter speed.** A fast shutter speed can produce a sharp image if enough photons are collected. However, images with too fast shutter speed will have a lot of noise. So the bottleneck is the response time of image sensors, which depends on their light-sensitivities.
- (3) **ISO setting.** ISO is the film speed indicating the sensitivity of an image sensor to light. However, for the same image sensor, a high ISO setting will involve a high level of noise. For different image sensors, high light-sensitivity means less light needed to make an exposure. Within the same ISO setting, image sensors with higher light-sensitivity can produce higher-quality images with lower noise than the ones with lower light-sensitivity.

Taking high-quality photos using hand-held devices under dim light, especially under extreme illumination conditions, is even more challenging. This has been a problem for users of consumer cameras for many years. In this paper, we design a new imaging framework for hand-held devices to handle this challenge, while no other hand-held image capture devices with equivalent capabilities have been demonstrated. We also propose a blind deblurring method with a novel image prior based on this new imaging system. The imaging system has a new sensor pattern by adding panchromatic (pan), or "clear" pixels without any color filters, to the conventional Bayer pattern. Since the pan pixels are sensitive to all wavelengths of visible light, they collect a significantly higher proportion of light striking the image sensor. Therefore, to capture high-quality images, they have a much shorter response time than current commercial image sensors. The remaining red, green, and blue pixels are then used to record color information of the scene. A new demosaicing algorithm is also proposed to restore full-resolution images from pixels on the sensor. The shutter speed of pan pixels is controllable to users, so we can have multiple images with different shutter speeds. We design two shutters for pan pixels in one shot: the first with a fast shutter speed and the second with a slow shutter speed, resulting in a sharp grayscale image and a blurred color image. Our imaging system is similar with the previous one using a blurred/noisy image pair [Yuan et al. 2007], but has superior features in alignment, shutter speed, and ISO setting.

Our deblurring algorithm works in a two-step MAP fashion to estimate blur kernels and deblurred images under a joint minimization. Since pan images conserve most of the clear gradients in the scene, it can significantly improve the kernel estimation by providing latent information. The deblurring is regularized by a combined image prior, including a statistical part that favors sharpness, and a novel spatial part that is powerful in ringing control. Ex-

periments under various conditions are conducted to demonstrate the performance of our method, and comprehensive evaluations are also carried out to compare with previous approaches. Our method provides a complete and well-concerted solution to camera shake, integrating the most advanced imaging system and the state-of-the-art deblurring method elegantly.

## 2. PREVIOUS WORK

Researchers have been endeavoring to improve the light sensitivity of electronic image sensors. Muramatsu [1989] developed an electronic imaging system that includes two sensors, wherein one has no color filters, and the other contains a pattern of color filters with an optical beam splitter. While this system improves the light sensitivity over a single conventional image sensor, the overall complexity, size, and cost are much higher. Furthermore, the beam splitter directs only half the light from the image to each sensor, limiting the improvement in photographic speed. The imaging system introduced by [Compton and Hamilton 2007] captures photos under varying lighting with one sensor, where some pixels have color filters, and the others do not. Since this system only uses a simple interpolation algorithm for image reconstruction, it may have imaging problems under dim light. Nayar and Narasimhan [2002] developed a multi-sampled imaging technique with a structural interpolation algorithm on assorted pixels. It can capture multiple dimensions of imaging such as spectrum, brightness, and polarization. The systems of [Susanu et al. 2009; Border et al. 2009] used a new sensor with light-sensitive pixels to capture high-quality images with a compensation processing step that can remove motion blurs caused by low lighting.

The image deblurring can be roughly classified into two categories: "blind" deblurring and "non-blind" deblurring. If the blur kernel is unknown, the problem is "blind", and vice versa. For non-blind deconvolution, a conventional technique is the Richardson-Lucy (R-L) deconvolution [1974], which computes the latent image with the assumption that its pixel intensities conform to a Poisson distribution. Recently, Levin et al. [2007] used a sparse prior for non-blind deconvolution, which was also referred to as the hyper-Laplacian prior by [Krishnan and Fergus 2009]. Their methods impressively improve the deblurring result by reducing ringing artifacts. In [Yuan et al. 2008], a progressive inter-scale and intra-scale approach was proposed, which is also featured in ringing control. Joshi et al. [2009] exploited color priors in non-blind image deconvolution, and applied them to deblurring and denoising.

Blind deblurring is an ill-posed problem. Recent work often gets aid from image priors. Fergus et al. [2006] showed that blur kernels are often complex and sharp. They adopted ensemble learning to recover a blur kernel while assuming a certain statistical distribution for natural image gradients as a prior. Shan et al. [2008] proposed a concatenation of two piece-wise continuous linear and quadratic functions to model image prior. Cai et al. [2009a] exploited the curvelet system for kernels and the framelet system for images to reduce the ill-posed problem to a joint optimization that maximizes the sparsity of the kernel and the sharp image. In [Cho and Lee 2009], a fast deblurring method was proposed by introducing a prediction step. The graphics processing unit (GPU) implementation accelerates the running speed of their algorithm. Levin et al. [2009] analyzed MAP failures in blind deconvolution, and evaluated single-image deconvolution algorithms using collected blur data with ground truth. Multiple blurred images can provide more information of the scene, which can reduce ambiguities of blind deblurring. Chen et al. [2008] developed an algorithm to deblur two consecutively-captured blurred photos from camera shake.

However, it requires accurate image alignment that is difficult to achieve for blurred images. Multiple images have more information than single images, but may also generate divergence of estimating. Cai et al. [2009b] relaxed this requirement by extremely sparse representation in the redundant curvelet system. It, however, still requires manual alignment of the images. For non-uniform deblurring, Whyte et al. [2010] proposed a parametrized geometric model in terms of the rotational velocity of the camera, and applied it to blind and non-blind deblurring.

We notice a new type of deblurring arising, which utilizes additional information captured by special camera systems to improve the deblurring. We call this type of deblurring as “Quasi-blind” deblurring. In [Ben-Ezra and Nayar 2003], a hybrid camera simultaneously captures a high-resolution image together with a sequence of low-resolution images that are temporally synchronized. Optical flow is derived from the low-resolution images to compute the global motion blur of the high-resolution image. Raskar et al. [2006] proposed a “fluttered shutter” camera with coded exposure, which opens and closes the shutter during a normal exposure time with a pseudo-random sequence. The moving object in their method was assumed to have constant velocity, and hence different exposure times lead to different sizes of blurring. This idea was extended to video that has frames with different exposure time by [Agrawal et al. 2009]. Yuan et al. [2007] proposed a method of deblurring with blurred/noisy image pairs. An image pair is captured in separated shots, including a blurred image under a long exposure, and a noisy image by a fast shutter. Due to short exposures under dim light, the noise may be severe, and thus the deblurring results are compounded with the performance of de-noising. In [Levin et al. 2007], a coded aperture was placed on a conventional camera to obtain a rough shape of defocus blur. Zhou and Nayar [2009] evaluated aperture patterns based on the quality of deblurring. In [2008], Levin et al. built a prototype camera that translates within its exposure following a parabolic displacement rule. Hence, blurs can be removed by deconvolving the entire image with an identical, known kernel. Joshi et al. [2010] attached gyroscopes and accelerometers to the camera, which can directly obtain the camera movement during exposure.

Our system in spirit belongs to this category, and it is similar to [Yuan et al. 2007] but fundamentally different on both imaging system and deconvolution method. The system in [Yuan et al. 2007] built on conventional cameras, has limitations in alignment, shutter speed, and ISO setting.

### 3. IMAGING SYSTEM

We now introduce our new image sensor and imaging system.

#### 3.1 Image Sensor

A digital imaging system uses an electronic sensor to create an electric representation of a visual image. Examples of such electronic image sensors include the charge-coupled device (CCD) sensor, and the active pixel sensor devices. The latter are often referred as Complementary Metal Oxide Semiconductor (CMOS) sensors because of the ability to fabricate them in a CMOS process. Typically, these image sensors include a number of light-sensitive pixels, often arranged in a regular pattern of rows and columns. For capturing color images, a pattern of filters is typically fabricated on the pattern of pixels with different filter materials, which make individual pixels sensitive to only a portion of the visible light spectrum such as Red, Green, and Blue, as shown in Fig. 1 (a). The color filters necessarily reduce the amount of light reaching each pixel, and

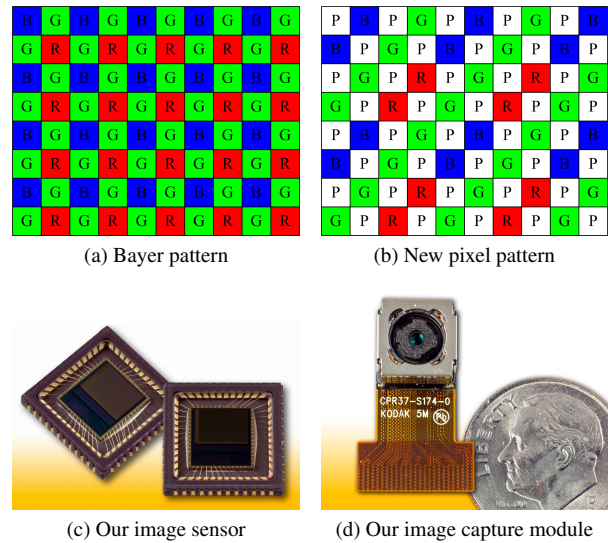


Fig. 1. A new image sensor and pixel pattern. R, G, B, and P stand for Red, Green, Blue, and Panchromatic pixels, respectively.

thereby reduce the light sensitivity of each pixel. A need persists for improving the light sensitivity of electronic color image sensors to permit images to be captured at lower light levels.

We use a new color image sensor with panchromatic pixels that have high light sensitivity, as shown in Fig. 1 (b). It includes four pixel arrays with color filters applied to three of the arrays to make each array sensitive to red, green, or blue, and with no color filter array applied to the fourth array (pan pixels). When an image is captured using this sensor, it is represented as a high-resolution, high-light-sensitivity monochrome image along with three low-resolution images corresponding to red, green, and blue, which have lower light-sensitivity. Because the pan pixels are added into the sensor, the charge leakage around each pixel is larger relative to the conventional Bayer pattern. During the design of the color filter array (CFA) of our new sensor, we also try to reduce the charge leakage problem to capture sharper and clearer images. Our new imaging sensor in Fig. 1 (b) is a CMOS sensor with 5M Pixels. In experiments, we use a hand-held camera system with this new image sensor.

#### 3.2 Image Demosaicing

A new demosaicing algorithm is designed to recover color images with full resolution from our image sensor. There is a large literature on demosaicing with Bayer patterns [Bayer 1976]. To reduce visual artifacts, the color differences between green/red and green/blue are interpolated in Bayer pattern demosaicing. By analyzing human visual perception, we use color difference interpolation between panchromatic pixels and RGB pixels to reduce visual artifacts. The procedure of our demosaicing algorithm is shown as follows:

- (1) **Noise removal.** We apply the sigma filter and the median filter to raw image-sensor data to remove the high frequency and impulse noise, as shown in Fig. 2 (a). For chromatic noise reduction, we let the average gradients of R, G, and B images equal to the average gradients of pan image to remove low-frequency chroma noise.

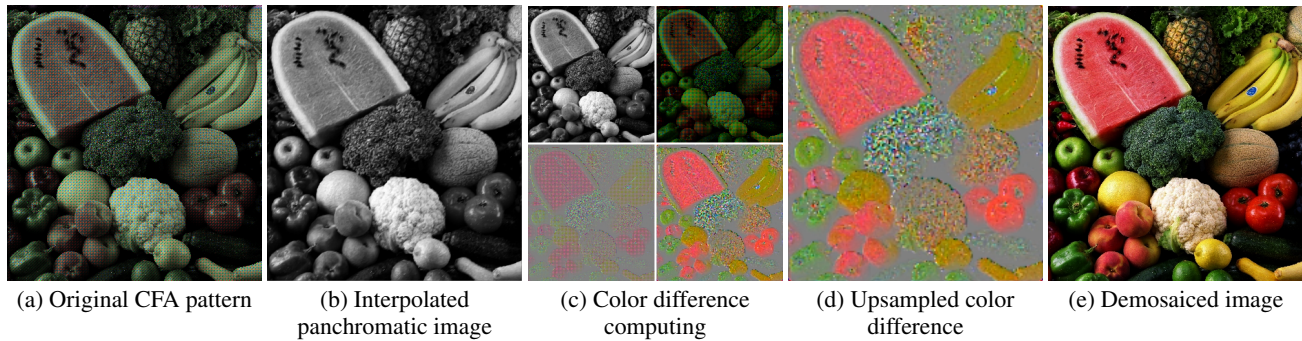


Fig. 2. Full-color image demosaicing with panchromatic pixels: (a) is the original CFA pattern from the new image sensor; (b) is the interpolated high resolution panchromatic image; (c) is the computing process of low-resolution color difference; (d) is upsampled high-resolution color difference; (e) is the high-resolution demosaiced image. In (c), there are the low-resolution panchromatic image in top-left, low-resolution Bayer pattern (Red, Green, and Blue) in top-right, color difference pattern between Bayer pattern and panchromatic image in bottom-left, and demosaicing color difference image in bottom-right. Zoom-in allows to see details of the CFA pattern.

- (2) **Pan image reconstruction.** We interpolate the monochrome image captured by pan pixels to get high-resolution grayscale image  $P$ , as shown in Fig. 2 (b).
- (3) **Bayer pattern interpolation.** We apply Bayer pattern CFA [Bayer 1976] to three single-channel RGB images to interpolate a color image in three channels in the low resolution.
- (4) **Color difference image computing.** We downsample pan pixels to get a low-resolution pan image, and extract R, G, and B from raw image-sensor data to get a low-resolution Bayer pattern. Then, we compute the color difference pattern by subtracting Bayer pattern from the pan image in each pixel. Finally, we apply a Bayer pattern demosaicing method to the color differences to get a full color difference image that has three channels (R-P, G-P, and B-P) in each pixel, as shown in Fig. 2 (c).
- (5) **Color difference image upsampling.** The high-resolution color difference image is then computed by upsampling as shown in Fig. 2 (d).
- (6) **Image demosaicing.** We combine the high-resolution pan image computed in Step (2) and upsampled color difference image computed in Step (5) to get the full-resolution color image as shown in Fig. 2 (e).

Using the new sensor and the demosaicing algorithm, we can simultaneously capture a full-resolution color image and a full-resolution grayscale image from pan pixels with high light-sensitivity, as shown in Fig. 2.

In the Bayer CFA pattern, the green pixels are usually used to provide the luminance information for the demosaiced image, while the red and blue pixels are used to provide the chrominance information. In our new pattern, the panchromatic pixels are used to provide the luminance information for the demosaiced image, and the red, green, and blue pixels are used to provide the chrominance information. The perception of image structure is largely determined by the response of the luminance channel of human visual system (HVS) [Alleysson et al. 2005]. In our pattern, there are half the number of red, green, and blue pixels as in the Bayer CFA pattern. However, they are used solely for chrominance demosaicing. The chrominance information is mostly low frequency from HVS perspective, so there is little to no “visual penalty” for subsampling the chrominance channels by a factor of two. It may be noticed that, the Foven X3 sensor has three photosites for each pixel that

respond to different wavelengths of light. It has a higher color resolution than the Bayer pattern sensor and our sensor, if the same number of pixels is used. However, our pan pixels have faster responding time. This feature is significant to our deblurring system.

#### 4. DEBLURRING WITH PAN PIXELS

This section details a method to capture high-quality images under dim light, using a hand-held device with our new image sensor.

##### 4.1 Problem Formulation

The image blurring is usually formulated as the convolution of the latent sharp image  $L$  and a blur kernel  $K$  with corresponding noise  $N$ , given by:

$$B = L \otimes K + N, \quad (1)$$

where  $B$  is the blurred image, and  $\otimes$  is the convolution operator. The goal of deblurring is to recover the latent image  $L$  from the blurred image  $B$ .

To achieve this goal, we devise two shutters in our imaging system, producing two images in one shot for dim light: one with shorter exposure and the other with longer exposure. The exposures can be set by users, and there is no gap between the two images. The image-pair mechanism has been adopted for deblurring as a concise and effective method in previous work. Fig. 3 compares some image-pair methods [Lim and Silverstein 2006; Yuan et al. 2007]. The integration time of red, green, and blue pixels is the total exposure time  $t = t_2$  with a slow shutter speed and a low ISO setting. The typical shutter speed of a blurred image in dim lighting is longer than 1 second. The panchromatic pixels are read out twice with different ISO settings and integration time during the entire exposure. At time  $t_1$ , the grayscale image  $P_1$  is read out by interpolating pan pixels with high ISO setting. We set  $t_1$  as a safe exposure time of pan pixels to make  $P_1$  sharp without blur. It may be noticed that,  $P_1$  has much lower noise and faster imaging speed ( $t_1 < (t_4 - t_3)$ ) than the noisy image in [Lim and Silverstein 2006; Yuan et al. 2007], because of the high light-sensitivity of the pan pixels. After time  $t_1$ , pan pixels are reset with low ISO and start to expose again. At time  $t_2$ , all pixels including red, green, blue, and pan pixels are read out. Using the image reconstruction algorithm described in Section 3.2, we can get a blurred grayscale image  $P_2$  and a blurred color image  $B$  at time  $t_2$ . Because the reset time of

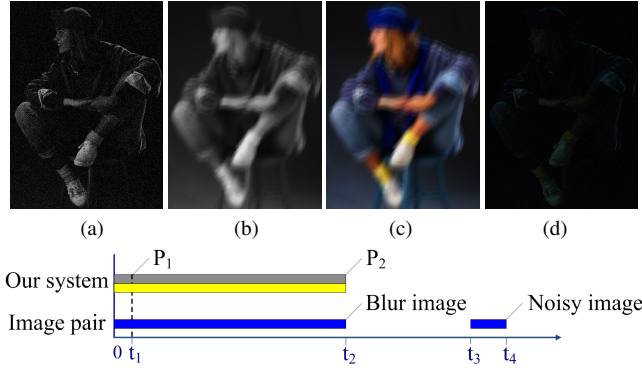


Fig. 3. Comparison between our imaging system and the image-pair systems introduced by [Lim and Silverstein 2006; Yuan et al. 2007]: (a) is a sharp grayscale image  $P_1$  with short exposure; (b) is a blurred grayscale image  $P_2$  with long exposure; (c) is a blurred color image  $B$ ; (d) is a noisy image used for the image pair system. The comparison between these two capture strategies in terms of timeline is shown in the bottom row. In our imaging system, the gray bar is the exposure of panchromatic pixels and the yellow bar is color pixels (red, green, and blue). In the image-pair systems, the blue bar is the exposure of pixels in the image sensor with two separate shots.

pan pixels is very short (usually 2-5 milliseconds), our method can capture a noisy sharp grayscale image  $P_1$ , a blurred color image  $B$ , and a grayscale image  $P_2$  with no alignment needed. In a sharp contrast, the methods using image pairs [Lim and Silverstein 2006; Yuan et al. 2007] need to sequentially capture a blurred image and a noisy image, with an extra work of alignment required.

## 4.2 Bayesian Deconvolution

Recent work [Fergus et al. 2006; Levin et al. 2007; Shan et al. 2008] has demonstrated that the probabilistic model is an effective tool for image deconvolution. In this model, the posterior is proportional to the product of conditional probability and prior probability, given by the Bayes' rule,

$$p(L, K|B) \propto p(B|L, K)p(L)p(K). \quad (2)$$

**Likelihood.** As a commonly-accepted assumption, the noise  $N$  is subject to the Gaussian distribution with zero-mean. While noise generation is much more complicated during image capture, we usually simplify it to be Gaussian. Therefore, we define the likelihood as a Gaussian-type function, given by

$$p(B|L, K) = e^{-(L \otimes K - B)^2}. \quad (3)$$

**Image prior.** The image prior expresses how we favor the deconvolved image after deconvolution. Conventional image priors usually consider the statistical distribution of intensities (mixture-of-Gaussian) or gradient magnitudes (heavy-tailed distribution). We propose a novel spatial distribution term, and design new our image prior as:

$$p(L) = p_t(L)p_p(L), \quad (4)$$

where  $p_t(L)$  denotes the statistical prior that presents the statistical distribution of gradient magnitudes of an image, and  $p_p(L)$  is the spatial prior that describes the spatial distribution of image gradients.

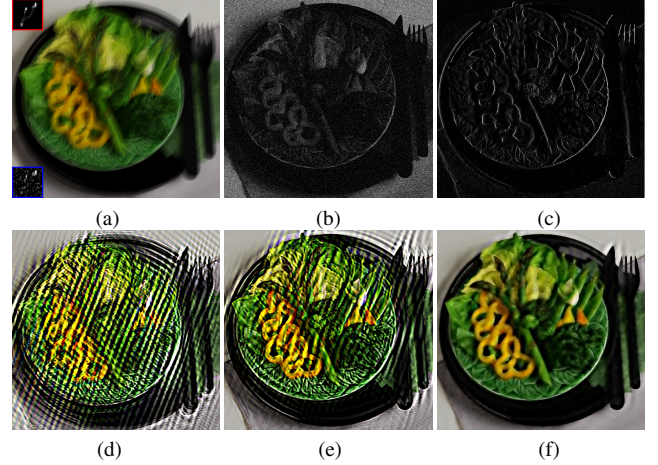


Fig. 4. The de-ringing effect of our spatial prior: (a) is a blurred image with the ground truth kernel (shown in the red box), and a noisy kernel (shown in the blue box) used for all three methods; (b) is our  $P$  image; (c) is x-derivative map of pan image  $P$ ; (d) is the deblurring result with the local prior in [Shan et al. 2008]; (e) is the result with the sparse prior in [Levin et al. 2007]; (f) is the result by our spatial prior only.

We adopt the sparse prior [Levin et al. 2007] as the representation of the statistic prior, given by

$$p_t(L) = e^{-\lambda_1 \sum_i (|\partial_x L_i|^\alpha + |\partial_y L_i|^\alpha)}, \quad (5)$$

where  $\lambda_1$  is a coefficient,  $i$  denotes pixel index, and  $\alpha$  is a positive exponent value set in the range of [0.5, 0.8] as suggested by [Levin et al. 2007; Krishnan and Fergus 2009].

Although the distributions of different images in the gradient magnitude domain are similar, we notice that they vary significantly in the spatial domain, and this is critical for the quality of deblurring. Therefore, we propose a new spatial prior that depicts how the deblurred image is favored spatially. The pan image  $P$  in our system conserves most of the clear gradients in the scene, from which we can estimate the spatial distribution of image gradients. Thus, we design our new spatial prior as

$$p_p(L) = e^{-\lambda_2 \sum_i (\partial_x L_i - \partial_x P_i)^2 + (\partial_y L_i - \partial_y P_i)^2}, \quad (6)$$

with coefficient  $\lambda_2$ . Since the  $P$  image is usually dim and noisy, we apply denoising and enhancement to it in a pre-processing stage.

This derivative-based spatial prior has a strong effect on de-ringing. Fig. 4 shows the de-ringing effect of our spatial prior compared with other de-ringing priors. We use a noisy kernel (shown in the blur box in Fig. 4 (a)) for deconvolution, which causes many ringing artifacts in (d) and (e). The spatial prior substantially reduces ringing artifacts.

**Kernel prior.** The kernel prior  $p(K)$  is commonly recognized as a sparsity prior with most values close to zero and all entries being positive. Therefore, we define our kernel prior served as regularization as a 1-norm of  $K$ :

$$p(K) = e^{-\lambda_3 \|K\|_1}, \quad \text{with } \sum_j k_j = 1, k_j \geq 0, \quad (7)$$

where  $\lambda_3$  is a coefficient,  $\|\cdot\|_l$  denotes the  $l$ -norm operator, and  $k_j$  denotes the entry of  $K$  with index  $j$ .

### 4.3 Estimation

A straightforward approach to solve the Bayesian inference is to find the MAP solution, which is equivalent to solving a regularized minimization problem. A primary concern of this approach is the local minimum that may trap the optimization. As analyzed in [Levin et al. 2009], even the global optimum of the MAP can not guarantee to find a desired sharp latent image with less ringing. Therefore, the key of using MAP is to get a good initial value. In this section, we will introduce how our system works on obtaining initial value and reaches high-quality estimation.

**Objective function.** By taking the negative logarithm of Eq. (2), the MAP problem transforms to a minimization problem, with the objective function defined as

$$J(L, K) = (L \otimes K - B)^2 + \lambda_1 \sum_i (|\partial_x L_i|^\alpha + |\partial_y L_i|^\alpha) + \lambda_2 \sum_i ((\partial_x L_i - \partial_x P_i)^2 + (\partial_y L_i - \partial_y P_i)^2) + \lambda_3 \|K\|_1. \quad (8)$$

We solve this joint minimization problem by a two-step estimation, i.e., to estimate the kernel first and then to estimate the latent image.

**Kernel estimation.** In our deconvolution system, we use the two grayscale images:  $P_1$  with short exposure and  $P_2$  long exposure to estimate the kernel. These two images are interpolated using the same algorithm, and  $P_2$  approximately has the same blur kernel with the interpolated full-color image. Therefore, we will use  $P_1$  and  $P_2$  to replace  $L$  and  $B$  in the kernel estimation. Since  $P_1$  is dim and noisy, we pre-process it by a bilateral filter [Tomasi and Manduchi 1998] and an inverse gamma correction.

For high-resolution images, a user-selected patch [Fergus et al. 2006] is adopted to speed up the computation. In our observation, the effects to estimate the kernel differ across regions. Smooth regions are more sensitive to noise, and rough regions with high deviation of intensity are more robust. Therefore, we select a region  $\Omega$  of pixels with large deviations of intensity for the estimation of the blur kernel. By fixing  $L$  and using  $P_1$  and  $P_2$ , this energy can be further simplified to

$$J(K) = (P_{1\Omega} \otimes K - P_{2\Omega})^2 + \lambda_3 \|K\|_1. \quad (9)$$

In our method, we simply apply the Laplace operator on blurry pan image  $P_2$ , and select the region  $\Omega$  as pixels with great values. This will make the estimation much more efficient than using the entire image.

A multi-scale approach is used for large kernels to avoid local minima during the optimization. At the coarsest scale, the estimation of  $K$  is initialized as a diagonal matrix. In other scales, previous estimation from the last scale is up-sampled to initialize  $K$  in the current scale. For most natural images with small blur, only one scale is sufficient to recover the accurate kernel. For a challenging case with large blur, 3-4 scales may be used. Between scales, we also eliminate small elements (e.g., less than 0.1 of the total energy) to reduce the noise of estimation.

**Estimation of the latent image.** By fixing  $K$  from Eq. (8), the objective function is reduced to

$$J(L) = (L \otimes K - B)^2 + \lambda_1 \sum_i (|\partial_x L_i|^\alpha + |\partial_y L_i|^\alpha) + \lambda_2 \sum_i ((\partial_x L_i - \partial_x P_{2i})^2 + (\partial_y L_i - \partial_y P_{2i})^2), \quad (10)$$

which is not convex. This problem can be solved by the iterative re-weighted least square (IRLS) method [Levin et al. 2007], or by the fast deconvolution method [Krishnan and Fergus 2009].

Table I. Shutter-speed and ISO settings in Fig. 5-8.

	Blurred image	Panchromatic image
Book (Fig. 5)	1.0s, ISO 100	1/100s, ISO 800
Toy (Fig. 6)	1.0s, ISO 100	1/80s, ISO 800
Hotel (Fig. 7)	1.3s, ISO 100	1/250s, ISO 1600
Fruit (Fig. 7)	1.6s, ISO 100	1/125s, ISO 1600
Family (Fig. 8)	2.0s, ISO 100	1/100s, ISO 1600
Berry (Fig. 8)	2.0s, ISO 100	1/100s, ISO 1600

Table II. Software parameters in experiments.

	Scales	$w$	$\sigma_d$	$\sigma_r$	$\lambda_1$	$\lambda_2$	$\lambda_3$
Book (Fig. 5)	1	5	3	0.1	0.01	0.6	0.1
Toy (Fig. 6)	1	5	3	0.1	0.01	0.8	0.1
Hotel (Fig. 7)	3	5	3	0.1	0.01	0.8	0.1
Fruit (Fig. 7)	3	5	3	0.1	0.01	0.4	0.1
Family (Fig. 8)	1	5	3	0.1	0.01	0.6	0.1
Berry (Fig. 8)	1	5	3	0.1	0.01	0.6	0.1

## 5. EXPERIMENTAL RESULTS

To demonstrate the performance of our system, we utilize a variety of images captured under low lighting environment using the new image sensor (CMOS, 5M Pixels). In experiments, we manually set all the camera parameters such as exposure time, aperture, focal length, and ISO. We set a safe exposure time for the first image (a noisy image) to make it sharp without blur. For the second image (a blur image), we also carefully set exposure time to make sure that it has no saturation. Table I documents shutter speeds and ISO settings used in experiments: Fig. 5-8. Table II details the software parameters in all experiments, including the number of scales in kernel estimation, window size ( $w$ ) of bilateral filter, space ( $\sigma_d$ ) and range ( $\sigma_r$ ) standard deviations in the bilateral filter, and  $\lambda_1$  to  $\lambda_3$  in Eq. (8). Previous methods [Lucy 1974; Fergus et al. 2006; Levin et al. 2007; Yuan et al. 2007; Shan et al. 2008; Cho and Lee 2009; Xu and Jia 2010] are used for comparison. Blurred and pan images used in Fig. 6-8 are shown in Fig. 9.

**Comparison with non-blind methods.** We first compare our method with three non-blind deconvolution methods, as shown in Fig. 5. To fairly and consistently compare all the methods, we apply our estimated kernel (shown in a red frame) to all other methods. The kernel sizes is  $25 \times 25$ . With the new spatial image prior, our deblurring result exhibits richer and clearer texture details with less ringing than other non-blind deconvolution methods.

**Comparison with blind methods.** We also compare our method with four recent blind deblurring methods, as shown in Fig. 6. From the results, we can see that [Fergus et al. 2006] and [Cho and Lee 2009] can not remove the blurs completely. [Shan et al. 2008] drives the results to excessive sharpness, accompanied by severe ringing artifacts. Both [Xu and Jia 2010] and our method produce nice deblurring results with no smear around the markers. As a trade-off for powerful suppression of ringing artifacts, our result looks a little smooth in the close-up. Our method also computed a very accurate blur kernel ( $31 \times 31$ ), comparing to the smears of markers in the blurred image given in Fig. 9.

**Large kernel.** To further examine the performance of our deblurring method together with our imaging system in more challenging cases, we conducted experiments on blur images with large blur and noise under extreme lightings. The primary challenge of large kernels is that they have much more dimensions than small kernels. We compare our result with other three methods, as shown in Fig. 7. For [Yuan et al. 2007], we make another shot with a fast shutter speed and high ISO settings on all pixels to obtain noisy



Fig. 5. Comparison of non-blind methods. From Left to Right: blurred/pan images, [Lucy 1974], [Shan et al. 2008], [Levin et al. 2007], and our method. We apply our estimated kernel to all other methods.



Fig. 6. Comparison with four blind methods. From Left to Right: [Fergus et al. 2006], [Shan et al. 2008], [Cho and Lee 2009], [Xu and Jia 2010], and our method. The blur kernel indicated by the smears of four black markers, is accurately estimated by our method.

color images. The low quality of noisy images and large blur kernels severely influence the deblurring of [Yuan et al. 2007]. Ringing and blurring artifacts can be found in the results of [Cho and Lee 2009] and [Xu and Jia 2010]. Our results are more clear, and have less ringing. The sizes of estimated kernels are  $83 \times 83$  and  $75 \times 75$ , with the image resolution  $1200 \times 1600$ .

**Large noise.** Finally, we conduct experiments on blurred images with high ISO settings (therefore, large noise) under very low lightings, as shown in Fig. 8. The kernel sizes are  $25 \times 25$  and  $21 \times 21$  for the two examples. Because of very dim lightings, the noisy images captured for [Yuan et al. 2007] are dark, and severely corrupted by noise, causing ringing artifacts and noise in their results. The panchromatic images, however, have higher quality, which greatly improves the deblurring results. Moreover, the residual deconvolution method used in Yuan's method involves noise by directly adding the detailed layer from the noisy image to the final result. It aggravates noise in the deblurring results. Our image prior has a smoothing effect, which produces less noise than [Cho and Lee 2009] and [Xu and Jia 2010].

## 6. DISCUSSION

The proposed deblurring method is built upon a new imaging system and a novel image prior. Despite the advantage of rapid-response pan pixels, our method has superiority at the algorithmic

front compared with previous image-pair method (i.e. [Yuan et al. 2007]). To examine this, we show an example of the two methods in Fig. 10. We adopt a blurred image and a pan image as a pair for the two methods. The blurred image is synthesized by a ground truth kernel shown in the corner, which eliminates the ambiguity of alignment. The estimated kernels by the two methods are very close to the ground truth, while our deblurring result has higher quality with less noise and ringing.

In this paper, we assume blurs are caused by in-plane camera shake, which is a limitation of our method. However, as shown by [Levin et al. 2009], the in-plane transition is often compounded with rotations in the third dimension, leading to spatially variant kernels. For a visual impression of this limitation, we show two examples of non-uniform blurs in Fig. 11. Each blurred image is synthesized by a ground truth kernel rotating in the third dimension, from  $0^\circ$  at the top to  $d^\circ$  at the bottom of a sharp image. Our method still works well at a small rotation that does not change the blur kernel much. For a large rotation, there is no uniform representation of the kernel, and therefore, the deblurring result has a lot of ringing artifacts.

Another limitation is that our image prior, though is powerful in ringing control, may introduce noise from pan images to deblurring results, as the result shown in Fig. 5. Therefore, pre-processing of denoising on pan images is unavoidable. Fortunately, this can hardly affect the kernel estimation, since the majority of

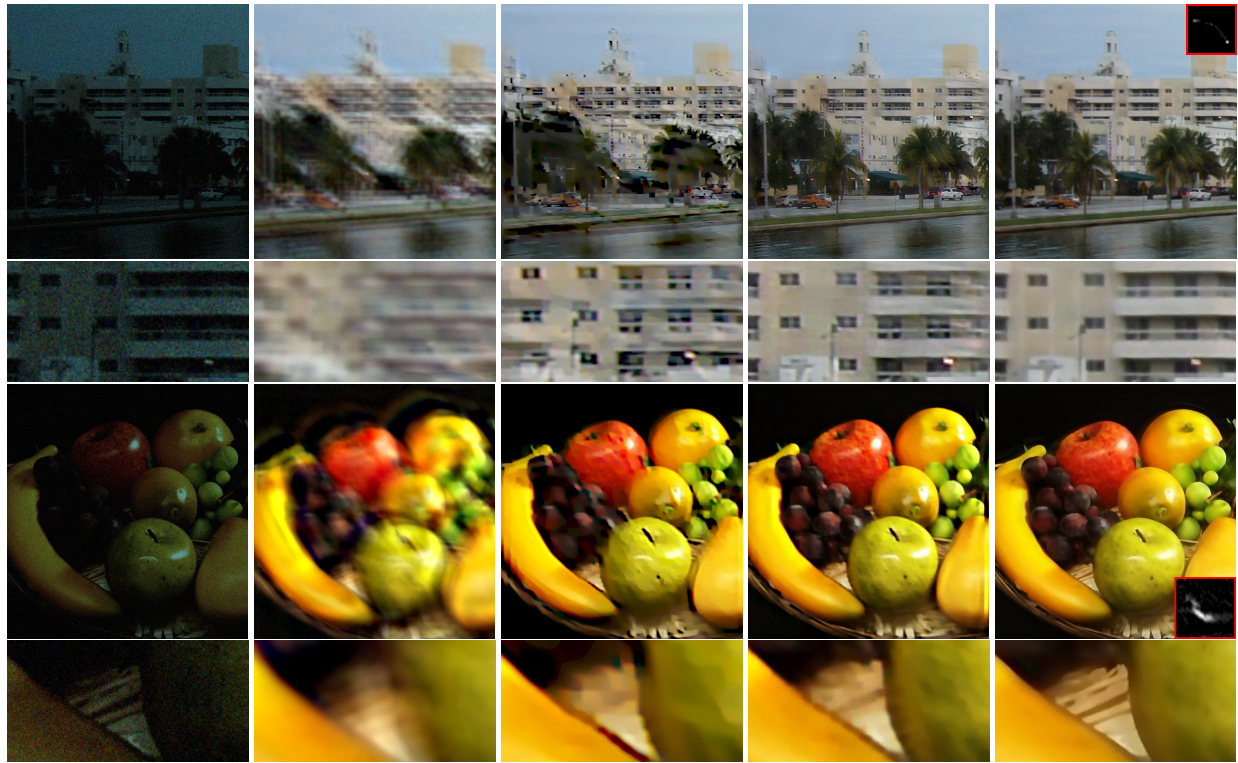


Fig. 7. Experiments on large kernels. From Left to Right: noisy images, [Yuan et al. 2007], [Cho and Lee 2009], [Xu and Jia 2010], and our method.

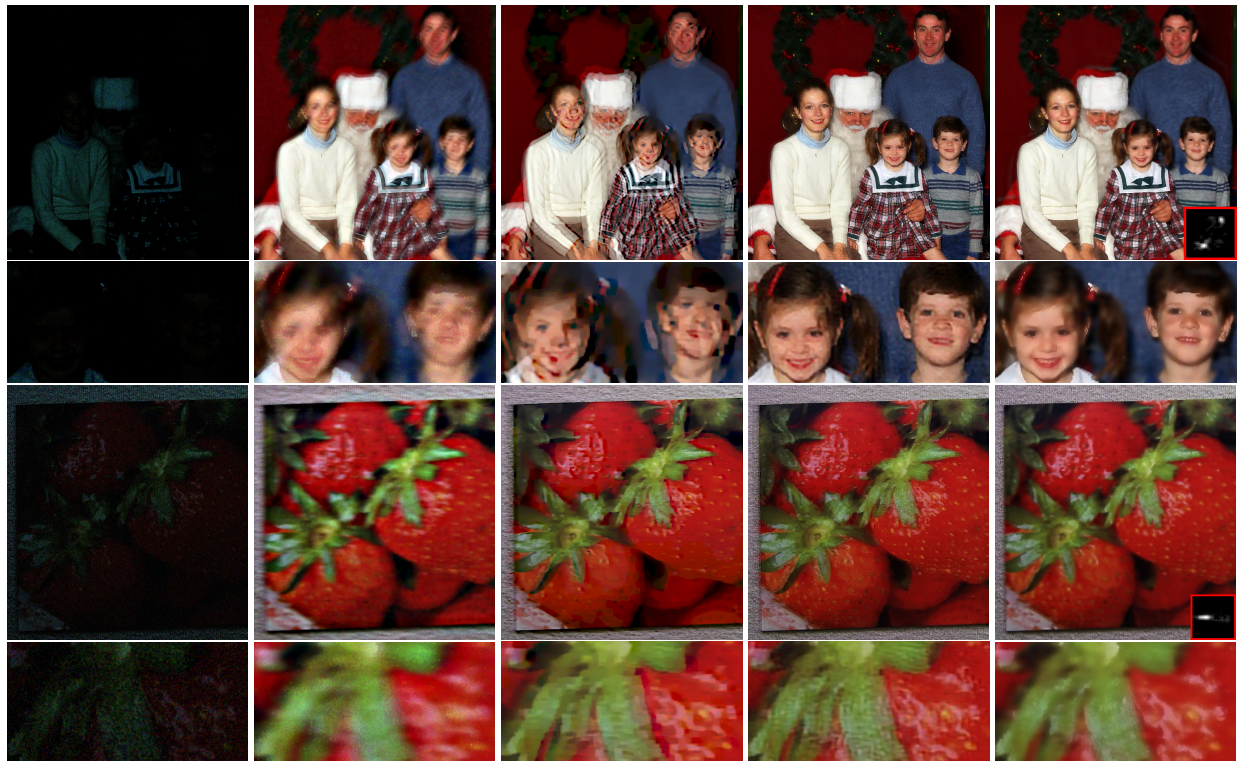


Fig. 8. Experiments on large noise. From Left to Right: noisy images, [Yuan et al. 2007], [Cho and Lee 2009], [Xu and Jia 2010], and our method.

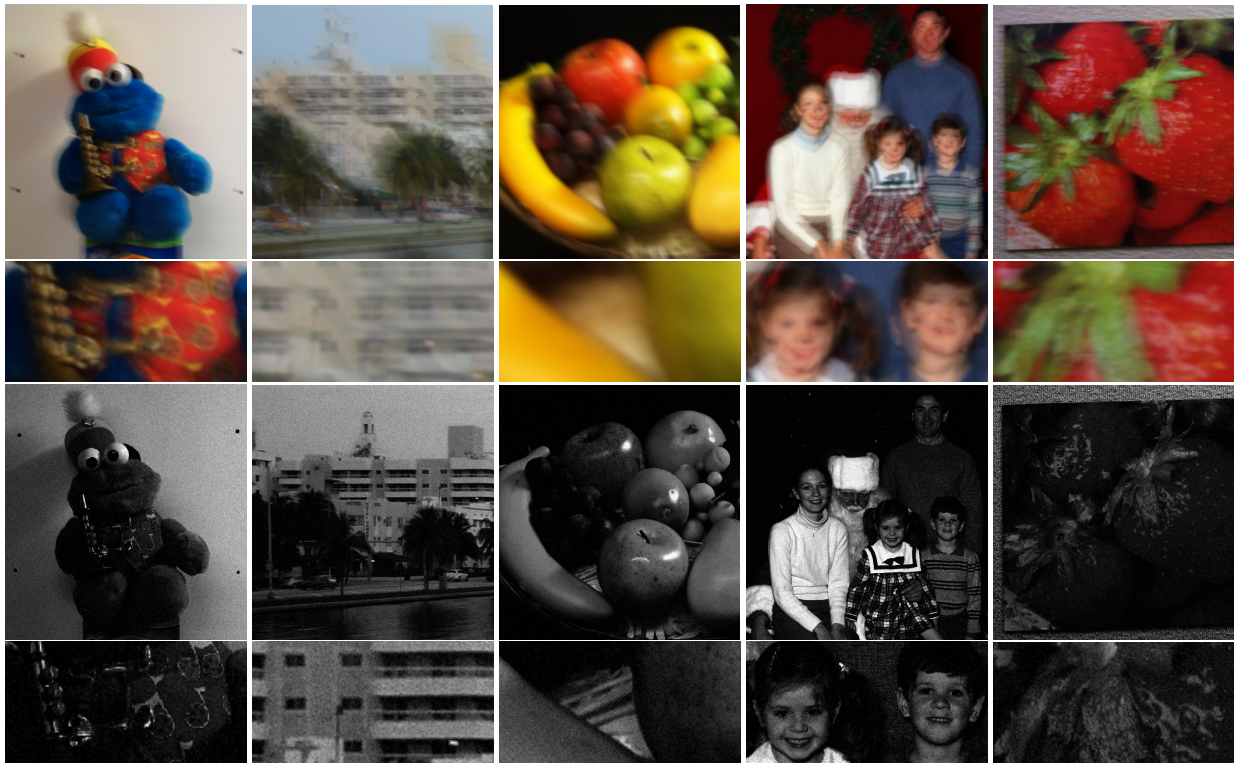


Fig. 9. Blurred and pan images used in experiments of Fig. 6-8.

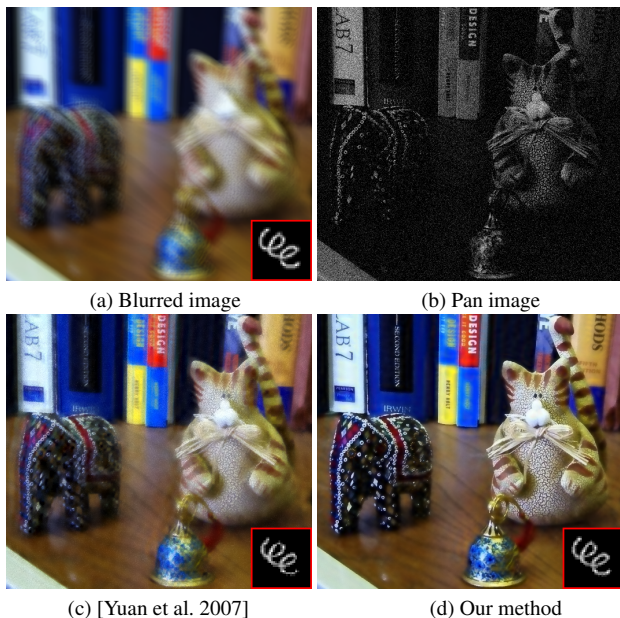


Fig. 10. Comparison with [Yuan et al. 2007] on the same data. The ground truth kernel and estimated kernels are respectively shown in the corners.

large derivatives are preserved after denoising. Moreover, our deblurring results have less noise than previous methods, as shown in Fig. 8.

## 7. CONCLUSION

We have articulated a high-quality image deblurring method built upon a new imaging system. High-light-sensitive pan pixels are fabricated to the image sensor, which have a fast response to image capture. Relative hardware and software are developed to assist the new sensor for image processing, such as charge leakage reducing, controllable shutter speed, image demosaicing with pan pixels, etc. At the algorithmic front, we design a novel image prior for suppressing ringing artifacts. The entire deblurring system has superior performance demonstrated in various experiments and comparisons. In the near future, we plan to extend the functionalities of our image deblurring system to overcome the limitations discussed above. We are also interested in employing our method in other closely-related applications such as video deblurring and out-of-focus deblurring.

## ACKNOWLEDGMENTS

This work could not have been completed without support of Kodak Research Lab (KRL). We would also like to thank all researchers in KRL who offered fruitful discussions and suggestions to the authors during this research work. In addition, Tingbo Hou and Hong Qin's research reported in this paper have been supported in part by US NSF grants: IIS-1047715, IIS-1049448, IIS-0949467, and IIS-0710819.

## REFERENCES

AGRAWAL, A., XU, Y., AND RASKAR, R. 2009. Invertible motion blur in video. *ACM Trans. Graph.* 28, 3, 95:1–95:8.



Fig. 11. Examples of spatially variant kernels. We rotate the ground truth kernel in the third dimension from  $0^\circ$  at the top to  $d^\circ$  at the bottom of a sharp image (a) to synthesize blurred images (c) and (e) with non-uniform blurs. The deblurring results are shown in (d) and (f), respectively. For a large spatially variant blur in (e), our deblurring result (f) has failed.

ALLEYSSON, D., SÜSTRUNK, S., AND HÉRAULT, J. 2005. Linear demosaicing inspired by the human visual system. *IEEE Trans. Image Processing* 14, 4, 439–449.

BAYER, B. 1976. Color imaging array. US Patent 3,971,065.

BEN-EZRA, M. AND NAYAR, S. 2003. Motion deblurring using hybrid imaging. In *Proc. Conf. Computer Vision and Pattern Recognition*. 657–664.

BORDER, J., ANDERSON, T., AND DEEVER, A. 2009. Determining and correcting for imaging device motion during an exposure. US Patent Application US2009/0021588A1.

CAI, J.-F., JI, H., LIU, C., AND SHEN, Z. 2009a. Blind motion deblurring from a single image using sparse approximation. In *Proc. Conf. Computer Vision and Pattern Recognition*. 104–111.

CAI, J.-F., JI, H., LIU, C., AND SHEN, Z. 2009b. High-quality curvelet-based motion deblurring from an image pair. In *Proc. Conf. Computer Vision and Pattern Recognition*. 1566–1573.

CHEN, J., YUAN, L., TANG, C.-K., AND QUAN, L. 2008. Robust dual motion deblurring. In *Proc. Conf. Computer Vision and Pattern Recognition*. 1–8.

CHO, S. AND LEE, S. 2009. Fast motion deblurring. *ACM Trans. Graph.* 28, 5, 145:1–145:8.

COMPTON, J. AND HAMILTON, J. 2007. Capturing images under varying lighting conditions. US Patent Application 2007/0046807A1.

FERGUS, R., SINGH, B., HERTZMANN, A., ROWEIS, S. T., AND FREEMAN, W. T. 2006. Removing camera shake from a single photograph. *ACM Trans. Graph.* 25, 3, 787–794.

JOSHI, N., KANG, S., ZITNICK, C. L., AND SZELISKI, R. 2010. Image deblurring using inertial measurement sensors. *ACM Trans. Graph.* 29, 4, 30:1–30:9.

JOSHI, N., ZITNICK, C. L., SZELISKI, R., AND KRIEGMAN, D. J. 2009. Image deblurring and denoising using color priors. In *Proc. Conf. Computer Vision and Pattern Recognition*. 1550–1557.

KRISHNAN, D. AND FERGUS, R. 2009. Fast image deconvolution using hyper-laplacian priors. In *Proc. Conf. Neural Information Processing Systems*.

LEVIN, A., FERGUS, R., DURAND, F., AND FREEMAN, W. T. 2007. Image and depth from a conventional camera with a coded aperture. *ACM Trans. Graph.* 26, 6, 70–77.

LEVIN, A., SAND, P., CHO, T. S., DURAND, F., AND FREEMAN, W. T. 2008. Motion-invariant photograph. *ACM Trans. Graph.* 27, 3, 71:1–71:9.

LEVIN, A., WEISS, Y., DURAND, F., AND FREEMAN, W. T. 2009. Understanding and evaluating blind deconvolution algorithms. In *Proc. Conf. Computer Vision and Pattern Recognition*. 1964–1971.

LIM, S. AND SILVERSTEIN, D. 2006. Method for deblurring an image. US Patent Application 2006/0187308A1.

LUCY, L. 1974. Bayesian-based iterative method of image restoration. *Journal of Astronomy* 79, 745–754.

MURAMATSU, A. 1989. Color video signal generating device using monochrome and color image sensors having different resolutions to form a luminance signal. US Patent 4,876,591.

NAYAR, S. K. AND NARASIMHAN, S. G. 2002. Assorted pixels: Multi-sampled imaging with structural models. In *Proc. European Conf. Computer Vision*. 472–479.

RASKAR, R., AGRAWAL, A., AND TUMBLIN, J. 2006. Coded exposure photography: motion deblurring using fluttered shutter. *ACM Trans. Graph.* 25, 3, 795–804.

SHAN, Q., JIA, J., AND AGARWALA, A. 2008. High-quality motion deblurring from a single image. *ACM Trans. Graph.* 27, 3, 73:1–73:10.

SUSANU, G., PETRESCU, S., NANU, F., CAPATA, A., AND CORCORAN, P. 2009. Rgbw sensor array. US Patent Application 2009/0167893A1.

TOMASI, C. AND MANDUCHI, R. 1998. Bilateral filtering for gray and color images. In *Proc. Int'l Conf. Computer Vision*. 839–846.

WHYTE, O., SIVC, J., ZISSERMAN, A., AND PONCE, J. 2010. Non-uniform deblurring for shaken images. In *Proc. Conf. Computer Vision and Pattern Recognition*. 491–498.

XU, L. AND JIA, J. 2010. Two-phase kernel estimation for robust motion deblurring. In *Proc. European Conf. Computer Vision*. 157–170.

YUAN, L., SUN, J., QUAN, L., AND SHUM, H.-Y. 2007. Image deblurring with blurred/noisy image pairs. *ACM Trans. Graph.* 26, 3.

YUAN, L., SUN, J., QUAN, L., AND SHUM, H.-Y. 2008. Progressive inter-scale and intra-scale non-blind image deconvolution. *ACM Trans. Graph.* 27, 3, 74:1–74:10.

ZHOU, C. AND NAYAR, S. K. 2009. What are good apertures for defocus deblurring? In *Proc. Int'l Conf. Computational Photography*. 1–8.

Received September 2008; accepted March 2009